





# A warning system for risk prediction of metabolic syndrome in a healthy population of blood donors

Simone Colombara <sup>1</sup>, Ilenia Epifani <sup>1</sup>, Alessandra Guglielmi <sup>1</sup>, and Ettore Lanzarone <sup>2</sup>

<sup>1</sup>*Department of Mathematics, Politecnico di Milano, Milan, Italy*

<sup>2</sup>*Department of Management, Information and Production Engineering, University of Bergamo, Dalmine (BG), Italy*

## Abstract

Metabolic syndrome is a complex clinical condition characterized by the simultaneous presence of multiple metabolic risk factors and represents a major public health concern. The syndrome develops silently and may remain undiagnosed for long periods, highlighting the importance of investigating early metabolic alterations before overt disease onset. Longitudinal monitoring of predominantly healthy individuals may help identify metabolic risk early. The paper proposes a Bayesian statistical model to estimate the probability of metabolic syndrome among blood donors during pre-donation screening, incorporating information collected at previous visits. Using longitudinal data from one of the main blood donor associations in Italy, AVIS Milan, we analyze repeated clinical and lifestyle measurements from a predominantly healthy population of donors. In particular, we fit a Bayesian multivariate model that jointly represents the logarithm of the five diagnostic components of metabolic syndrome. The model accounts for within-donor dependence across repeated visits and provides probabilistic estimates of individual risk. Our framework aims to provide clinicians at AVIS Milan with an interpretable traffic-light warning system (low, intermediate, high risk) during pre-donation screening to facilitate the identification of individuals at risk of metabolic syndrome at future visits and to support targeted preventive interventions during routine donor assessment, ultimately contributing to a long-term reduction in healthcare costs for the Italian national healthcare system.

**Key words:** Bayesian multivariate mixed-effects models, posterior predictive inference, longitudinal data, low-prevalence population, onset prediction, traffic-light classification

# 1 Introduction

Metabolic syndrome (MetS) is a complex clinical condition characterized by the simultaneous presence of multiple metabolic abnormalities, including abdominal obesity, elevated blood pressure, high fasting glucose, elevated triglycerides, and low levels of HDL cholesterol, which occur together and increase the risk of cardiovascular disease, type 2 diabetes, stroke, and mortality. [Noubiap et al. \(2022\)](#) estimates an increase of MetS prevalence of 3.4% every ten years, reaching over 31.5% prevalence in 2020s in the WHO European Region. Beyond its clinical severity, this trend imposes an economic burden on public health expenditures driven by MetS-associated conditions such as obesity and diabetes. Globally, direct health expenditure for diabetes surpassed 1 trillion US\$ in 2024 ([International Diabetes Federation, 2025](#)), while the economic impact of obesity is projected to exceed 4 trillion US\$ annually by 2035 ([World Obesity Federation, 2023](#)). To mitigate this load on health and public expenditure, developing data-driven tools for early screening and prevention of MetS is an urgent public health priority.

There are several definitions of MetS provided by different organizations, e.g., the International Diabetes Federation (IDF) and the National Cholesterol Education Panel-Adult Treatment Panel III (NCEP-ATP III) ([Grundy et al., 2005](#); [Alberti et al., 2006](#); [Kassi et al., 2011](#)). While they share a common conceptual framework, they differ in diagnostic thresholds and sometimes include ethnicity-specific criteria. In this study, we adopt the NCEP-ATP III definition of MetS, according to which a diagnosis is established when at least three of the conditions in [Table 1](#) are met. These factors, often related to insulin resistance, significantly increase the risk of developing serious chronic diseases ([Isomaa et al., 2001](#); [Najarian et al., 2006](#); [Air and Kissela, 2007](#)).

<b>Component</b>	<b>Men</b>	<b>Women</b>
Waist circumference ( <i>cm</i> )	> 102	> 88
Systolic Blood pressure ( <i>mmHg</i> )	$\geq 130$	$\geq 130$
Fasting Glucose ( <i>mg/dL</i> )	$\geq 100$	$\geq 100$
Triglycerides ( <i>mg/dL</i> )	$\geq 150$	$\geq 150$
HDL cholesterol ( <i>mg/dL</i> )	< 40	< 50

Table 1: MetS components according to the NCEP-ATP III definition, and diagnostic criteria. The diagnosis of MetS is established when at least three of the conditions are met.

MetS often develops silently, with few or no symptoms in its early stages, and is rarely the primary focus of clinical screening. Consequently, despite its clinical relevance, MetS and its individual components can remain undiagnosed for long periods. On the contrary, risk prediction of MetS in healthy individuals represents an important step toward preventing more serious diseases and implementing lifestyle changes to reduce their risk. Preventive measures such as dietary changes, increased physical activity, and weight management have been shown to effectively reduce

the impact of MetS.

However, data-driven early diagnosis of MetS remains challenging, as most available health data pertain to individuals who have already developed the disease. In contrast, data on healthy individuals before disease onset are scarce and accessible only in a few specific facilities. One such facility is a blood collection center, where healthy volunteers donate blood and undergo detailed blood tests over the course of years. Typical eligibility criteria for blood donation exclude individuals with severe cardiovascular or systemic diseases; therefore, blood donors are often considered a representative sample of a healthy adult population. For this reason, blood donors have also been used as a reference group in comparative studies between healthy and clinical populations (Roer et al., 2025). Nonetheless, evidence from cross-sectional studies shows that components of MetS, including abdominal obesity, dyslipidemia, impaired fasting glucose, and elevated blood pressure, are also present among blood donors (Peffer et al., 2015). Potential cardiovascular and metabolic effects of blood donation itself, particularly with respect to iron metabolism, have also been investigated, but the evidence remains inconclusive or contradictory (Salonen et al., 1998; Ascherio et al., 2001; Germain et al., 2013; Peffer et al., 2015). A recent systematic review found no strong evidence for a clear association between frequent blood donation and a reduced risk of MetS-related diseases (Quee et al., 2022). Overall, blood donation settings provide a relevant context for investigating metabolic risk in predominantly healthy individuals.

## 1.1 Our contribution

This paper proposes a Bayesian statistical model to estimate the probability that a blood donor exhibits MetS during the pre-donation check-up, using information collected at previous visits. We analyze a large longitudinal dataset from one of the main blood donor associations in Italy, namely the Milan department of the *Associazione Volontari Italiani del Sangue*, hereafter referred to as AVIS Milan, which integrates repeated clinical measurements and lifestyle data. Building on this rich and well-characterized data source, we propose a Bayesian multivariate modeling framework that jointly represents (the logarithm of) the five diagnostic components of MetS in Table 1.

The model accounts for within-donor dependence across repeated visits and provides probabilistic estimates of individual risk. The data structure enables investigation of the early dynamics and interactions among metabolic risk factors in a predominantly healthy population, offering insights not achievable in more clinically compromised cohorts. A distinctive feature of this study is that, to facilitate clinical interpretation and practical use, these probabilistic outputs are translated into an interpretable “traffic-light” warning system for risk stratification. Leveraging the posterior predictive distribution of the Bayesian model, each donor is classified into low, intermediate, or high

risk of meeting the diagnostic criteria for MetS at the next donation. This system translates complex statistical output into a practical tool that AVIS Milan clinicians can easily use, supporting real-time identification of at-risk individuals and guiding the need for further clinical investigation or early preventive intervention during routine donor check-ups.

Currently, in the blood donation setting, MetS evaluation during pre-donation screening is based on information collected at the current visit, along with data from previous visits and blood tests. However, this approach mainly reflects the donor’s current condition and lacks a forward-looking perspective, which is essential for early risk detection and prevention. Routine screenings are low-cost, and by focusing clinical time on at-risk donors during check-ups, early interventions can be encouraged while reducing overall healthcare costs.

Nonetheless, the findings of this study have broader applicability and may aid in screening healthy individuals across different contexts, offering a novel contribution to the existing literature. Note that the model we consider here has been specifically built for the AVIS Milan MetS data. Extensive efforts have been made to *best* represent the temporal dependence and the significance of other covariates for the five longitudinal MetS components. Alternative model specifications and dependence structures were evaluated using Bayesian predictive criteria; further details are provided in Appendix B.

## 1.2 Related work

To our knowledge, research on MetS in blood donors is largely cross-sectional and descriptive, with few studies leveraging large-scale longitudinal data with repeated measurements over extended follow-up periods, as in this paper. Methodologically, the study of MetS requires models that jointly capture multiple correlated biomarkers measured over time. Its diagnostic components (see Table 1) are biologically interconnected and driven by common pathophysiological processes. Analyzing them separately with univariate models assumes independence and may fail to fully exploit their joint dynamics (Rizopoulos et al., 2014); see also Regitz-Zagrosek et al. (2016) for related considerations in the cardiovascular literature. Longitudinal modeling strategies for early disease detection based on repeated biomarker measurements have been investigated by Han et al. (2020) for at-risk ovarian cancer patients, although primarily in univariate settings.

In parallel, machine learning (ML) approaches (e.g., decision trees, random forests, gradient boosting, and deep learning architectures) have been widely applied to the prediction and classification of MetS, typically formulating a diagnosis of MetS as a supervised classification problem based on cross-sectional data (e.g., Park et al., 2021; Kim et al., 2022; Sghaireen et al., 2022; Shin et al., 2023), not always considering blood donor cohorts or other healthy populations, or invasive

biomarkers. A notable advance is the multitask deep learning model by [Lee et al. \(2024\)](#), which jointly predicts MetS and its components using data from a large cohort (the Korean Genome and Epidemiology Study - KoGES, over 70,000 adults) and outperforms standard classifiers. However, it remains primarily predictive, relies on dichotomized outcomes, lacks explicit modeling of longitudinal correlations, requires substantial tuning, and offers limited uncertainty quantification.

To our knowledge, few ML studies incorporate time. Existing approaches, such as the visit-pair framework by [Tavares et al. \(2022\)](#), use data from one visit to predict outcomes at the next visit but do not capture the full joint evolution of biomarkers across repeated measurements. Other recent ML works ([Yang et al., 2022](#); [Goldman et al., 2025](#)) focus on identifying key risk factors that trigger the onset of the syndrome by selecting cohorts of initially healthy individuals and predicting their binary clinical status at the final visit.

Overall, while ML approaches – including multitask deep learning – achieve strong predictive performance, they mainly emphasize classification accuracy, provide limited probabilistic interpretation, and do not explicitly capture the joint temporal dynamics of MetS components. These limitations motivate the use of Bayesian multivariate longitudinal models for risk stratification, uncertainty quantification, and early screening in repeatedly monitored healthy populations.

Bayesian generalized linear mixed models (GLMMs) offer a flexible and well-established framework for jointly modeling multiple longitudinal biomarkers. Early work ([Zeger and Karim, 1991](#)) introduced Bayesian GLMMs via Gibbs sampling, later extended to multivariate and longitudinal settings (e.g., [Xu and Zeger, 2001](#); [Dunson, 2003](#); [Cai and Dunson, 2006](#)). Despite these advances, such models have rarely been applied to MetS, where its inherently multivariate and longitudinal nature is often simplified or overlooked. An approach similar to ours, namely assuming a Bayesian screening algorithm that incorporates the longitudinal trajectories of multiple non-invasive biomarkers into the calculation of the posterior risk of having hepatocellular carcinoma, is described in [Tayob et al. \(2022\)](#). The problem considered there is the early detection of disease in at-risk patients, using a personalized threshold for binary classification based on multiple biomarkers.

### 1.3 Organization of the paper

The paper is structured as follows. Section 2 presents the dataset and preprocessing steps. Section 3 introduces the Bayesian multivariate mixed-effects model. Section 4 describes the traffic-light risk classification system. Posterior inference is discussed in Section 5, followed by traffic-light prediction in Section 6. Section 7 compares our model with alternative ML approaches. Section 8 concludes the paper and outlines directions for future research. Appendix A presents the ex-

ploratory data analysis, details the imputation procedure for missing covariates, and describes the within-MCMC treatment of missing *waist* circumference values. Appendix B reports the alternative model specifications and dependence structures considered during model development. Finally, Appendix C illustrates the performance of the proposed model on a simulated dataset.

## 2 Data

We consider data from AVIS Milan, one of the largest voluntary blood donor organizations in Italy. The dataset integrates clinical records with self-reported lifestyle information. Data sources include the EMONET medical database (mandatory for the Regional healthcare system), which contains information on donations and clinical exams for each donor, and the organizational AVIS Milan dataset, which contains information on donors' lifestyles. We select donors who made at least four donations between January 2019 and September 2023 to ensure sufficient data for parameter estimation in our longitudinal model. Blood donors are subject to strict eligibility criteria, including minimum age requirements, body-weight thresholds, and acceptable ranges for physiological parameters such as blood pressure and hemoglobin concentration (Epifani et al., 2025).

According to Italian regulations, the minimum interval between two consecutive donations is 90 days for men and post-menopausal women and 180 days for other women, with limited flexibility after clinical evaluation. The five target variables shown in Table 1, excluding *waist circumference*, had missing rates below 1%, and donors with missing values in these variables were excluded. The dataset we consider here includes 11,556 visits across  $I = 2,228$  donors (1,907 men and 321 women). However, *waist circumference* is missing in 48.5% of the visits, but these values are included as latent parameters in the Bayesian model described in Section 3. In this cohort, the average interval between consecutive visits is 291 days for men and 339 days for women. These longer time gaps partly reflect the analysis of a time window that overlaps with the COVID-19 pandemic, which partially disrupted donation schedules. The original NCEP-ATP III definition of MetS also included a threshold for diastolic pressure. However, in this paper, we consider only systolic blood pressure ( $P_{MAX}$ ) rather than diastolic blood pressure, since the two are highly correlated and including both would result in redundant information. This modification was discussed with AVIS Milan clinicians, who deemed it consistent with MetS characteristics and with the study's objective.

Since we adopt a validation approach in this paper, we split the data into training and test sets. Specifically, for each donor, we allocate all observations, except the last one, to the training set and

the most recent observation to the testing set. We then compute in-sample posterior predictive distributions of the five target variables at the last donation. Accordingly, the training set includes 9,338 multivariate measurements, while the test set contains 2,228 observations (one per donor), 710 of which have no missing values for *waist circumference*. Exploratory data analysis on the training set is reported below.

The initial dataset comprises 39 variables, including the five MetS targets. We first removed covariates with high collinearity or missingness exceeding 50% (see Figure A.2). We assessed associations between covariates using chi-squared tests for categorical variables and empirical Pearson correlations for numerical variables. Based on this exploratory analysis, we removed the variables *hematocrit*, *MCV* (mean corpuscular volume), and *weight* to mitigate multicollinearity. Among categorical variables, *smoking* and *alcohol* were discarded due to high missing rates and strong associations with other categorical predictors. See Appendix A.1 for additional details. The blood group variables *Rh* and *ABO*, which showed limited predictive value for the metabolic targets (see Table A.4), were excluded from the dataset. We selected interaction terms using boxplots and Kruskal-Wallis tests between numerical and categorical covariates. The final multivariate longitudinal model includes 34 covariates and interaction terms, as reported in Table 2 along with their units of measure. See Appendix A.1 for details, in particular Figure A.1 shows the barplot of the donation counts for the training set.

We have applied the logarithmic transformation to the five target variables and to the covariates *alanine ALT* and *ferritin* to mitigate their right skewness (see Figure A.3). Before fitting the model, we standardized the target variables and all numerical covariates. Table 3 reports a summary of the five target variables in the dataset before log-transformation and standardization. The final set of covariates contains missing values, though all lower than 50% (percentages of NA shown in Table 2). Therefore, we have imputed missing values for these covariates, using multiple imputation by chained equations, i.e., the R package MICE (Van Buuren and Groothuis-Oudshoorn, 2011).

The empirical prevalence of MetS in the training set is 9.3% when considering only complete observations (i.e., excluding those with missing *waist circumference*). Across the entire training set, the overall prevalence drops to 7.2%. This lower figure represents a conservative estimate: for observations lacking *waist circumference*, a positive MetS diagnosis is defined only if at least three of the remaining four clinical criteria exceed their respective thresholds, effectively treating borderline cases as negative.

Covariates	Empirical Mean $\pm$ SD	NA (%)
<b>Demographics</b>		
Age	48.0 $\pm$ 9.96 <i>years</i>	0.0
<i>sex</i>	Men 86% (1907 donors); Women 14% (321 donors)	0.0
Height	175.8 $\pm$ 7.68 <i>cm</i>	0.2
<i>physical activity</i> (Active/Inactive)	Active: 67%; Inactive: 33%	46.7
BMI	25.4 $\pm$ 3.29 $\frac{kg}{m^2}$	0.2
<b>Measured by clinician</b>		
Heart Rate	67.1 $\pm$ 7.05 <i>bpm</i>	0.1
<b>Blood tests</b>		
Hemoglobin	14.9 $\pm$ 0.97 $\frac{g}{dL}$	0.1
Total Proteins	7.1 $\pm$ 0.40 $\frac{g}{dL}$	22.9
Creatinine	1.0 $\pm$ 0.15 $\frac{mg}{dL}$	21.8
Ferritin	65.4 $\pm$ 48.91 $\frac{ng}{mL}$	17.1
Platelets	236.2 $\pm$ 48.02 $\frac{10^3}{\mu L}$	0.1
Lymphocytes	32.9 $\pm$ 6.87 (%)	0.1
Eosinophils	2.8 $\pm$ 1.97 (%)	0.1
Basophils	0.8 $\pm$ 0.32 (%)	0.1
Monocytes	9.0 $\pm$ 1.82 (%)	0.1
MCH	29.3 $\pm$ 1.62 $\frac{pg}{cell}$	0.1
MCHC	32.7 $\pm$ 0.98 $\frac{g}{dL}$	0.1
WBC	5.9 $\pm$ 1.30 $\frac{10^3}{\mu L}$	0.1
Blood Volume Distribution (%)	13.1 $\pm$ 0.89	0.1
ALT	21.4 $\pm$ 11.34 $\frac{units}{L}$	22.7
<b>Interactions</b>		
ALT $\times$ <i>sex</i>	Men: 22.09 $\pm$ 11.40 $\frac{units}{L}$ ; Women 16.68 $\pm$ 9.71 $\frac{units}{L}$	22.7
Age $\times$ <i>sex</i>	Men: 47.63 $\pm$ 9.72 <i>years</i> ; Women 50.24 $\pm$ 11.20 <i>years</i>	0.0
BMI $\times$ <i>sex</i>	Men: 25.56 $\pm$ 3.15 $\frac{kg}{m^2}$ ; Women 24.00 $\pm$ 3.84 $\frac{kg}{m^2}$	0.2
Creatinine $\times$ <i>sex</i>	Men: 1.03 $\pm$ 0.14 $\frac{mg}{dL}$ ; Women 0.81 $\pm$ 0.12 $\frac{mg}{dL}$	21.8
Ferritin $\times$ <i>sex</i>	Men: 67.91 $\pm$ 50.32 $\frac{ng}{mL}$ ; Women 48.74 $\pm$ 33.91 $\frac{ng}{mL}$	17.1
Height $\times$ <i>sex</i>	Men: 177.39 $\pm$ 6.47 <i>cm</i> ; Women 164.56 $\pm$ 5.80 <i>cm</i>	0.2
Heart Rate $\times$ <i>sex</i>	Men: 66.93 $\pm$ 7.07 <i>bpm</i> ; Women 68.08 $\pm$ 6.87 <i>bpm</i>	0.1
Hemoglobin $\times$ <i>sex</i>	Men: 15.04 $\pm$ 0.85 $\frac{g}{dL}$ ; Women 13.52 $\pm$ 0.75 $\frac{g}{dL}$	0.1
Lymphocytes $\times$ <i>sex</i>	Men: 32.63 $\pm$ 6.84 (%); Women 34.51 $\pm$ 6.85 (%)	0.1
MCH $\times$ <i>sex</i>	Men: 29.30 $\pm$ 1.63 $\frac{pg}{cell}$ ; Women 29.39 $\pm$ 1.63 $\frac{pg}{cell}$	0.1
<i>physical activity</i> $\times$ <i>sex</i>	Active Men: 33.51%; Active Women: 33.38%	46.7
Platelets $\times$ <i>sex</i>	Men: 233.66 $\pm$ 47.01 $\frac{10^3}{\mu L}$ ; Women 253.53 $\pm$ 51.36 $\frac{10^3}{\mu L}$	0.1
Blood Volume Distribution $\times$ <i>sex</i>	Men: 13.02 $\pm$ 0.88 (%); Women 13.28 $\pm$ 0.92 (%)	0.1
WBC $\times$ <i>sex</i>	Men: 5.88 $\pm$ 1.29 $\frac{10^3}{\mu L}$ ; Women 5.95 $\pm$ 1.40 $\frac{10^3}{\mu L}$	0.1

Table 2: Covariate and interaction terms (34 total) included in (2), with summary statistics. For numerical covariates, we report the empirical mean  $\pm$  SD; for categorical covariates, we report the empirical frequency. The last column reports the percentage of missing values (NA) for each feature. Missing values are excluded from the computation of the empirical statistics.

Targets	Empirical Mean $\pm$ SD
<b>Measured by clinician</b>	
<i>waist circumference</i>	93.85 $\pm$ 10.26 <i>cm</i>
<i>PMAX</i>	121.89 $\pm$ 11.18 <i>mmHg</i>
<b>Blood tests</b>	
<i>glucose</i>	91.92 $\pm$ 10.60 $\frac{mg}{dL}$
<i>HDL cholesterol</i>	56.51 $\pm$ 14.20 $\frac{mg}{dL}$
<i>triglycerides</i>	105.51 $\pm$ 55.49 $\frac{mg}{dL}$

Table 3: Empirical means and standard deviations of the five target variables in the definition of MetS. Missing values in the *waist circumference* are excluded from the computation of these statistics.

### 3 Bayesian multivariate modeling of longitudinal MetS biomarkers

As mentioned in the Introduction, joint modeling of the five components of MetS is crucial since they are biologically interconnected risk factors. Modeling each component separately would overlook their inherent dependence, potentially leading to inefficient or biased inference, as noted in the context of cardiovascular diseases in [Regitz-Zagrosek et al. \(2016\)](#) and [de Bakker et al. \(2025\)](#). In particular, because we model the logarithms of the five MetS biomarkers across repeated donations with donor random effects, our model can be interpreted as a GLMM.

Let  $\mathbf{Y}_{ij} = (Y_{ij}^{(1)}, \dots, Y_{ij}^{(K)})'$  denote the column vector of the  $K = 5$  continuous outcome variables for individual  $i = 1, \dots, I$  at visit  $j = 1, \dots, n_i$ , corresponding to the five log-transformed and standardized MetS components. Note that the  $j$ th visit for the  $i$ th donor does not typically occur at the same time as the  $j$ th visit for the  $i'$ th donor, since donation timing depends on voluntary donor participation as well as the mandatory deferral period during which the donor is not eligible to donate again. At each visit  $j$ , an associated column covariate vector  $\mathbf{x}_{ij} = (x_{ij1}, \dots, x_{ijP})' \in \mathbb{R}^P$  is observed for donor  $i$ . The  $P$  covariates include demographic characteristics, anthropometric indices, lifestyle variables, hematological and biochemical markers, together with selected interaction terms, as reported in [Table 2](#). Age at each visit is included as a time-varying covariate, thereby allowing the model to account for calendar time across donations.

We specify the following multivariate Bayesian mixed-effects model:

$$\mathbf{Y}_{ij} \mid \boldsymbol{\mu}_{ij}, \boldsymbol{\Sigma}_{\mathbf{Y}} \stackrel{\text{ind}}{\sim} \mathcal{N}_K(\boldsymbol{\mu}_{ij}, \boldsymbol{\Sigma}_{\mathbf{Y}}), \quad i = 1, \dots, I, \quad j = 1, \dots, n_i, \quad (1)$$

$$\boldsymbol{\mu}_{ij} = \mathbf{x}'_{ij}\boldsymbol{\beta} + \mathbf{b}_i, \quad (2)$$

where  $\boldsymbol{\beta} := [\boldsymbol{\beta}^{(1)}, \dots, \boldsymbol{\beta}^{(K)}] \in \mathbb{R}^{P \times K}$  is the matrix of regression coefficients, and  $\mathbf{b}_i \in \mathbb{R}^K$  is a donor-specific random intercept vector. Each column  $\boldsymbol{\beta}^{(k)} = (\beta_{1k}, \dots, \beta_{Pk})'$  of  $\boldsymbol{\beta}$  represents the regression parameters associated with  $\mathbf{x}_{ij}$  on the  $k$ -th target outcome  $Y_{ij}^{(k)}$ . Thus, each of the five target variables depends on all  $P$  covariates, but with outcome-specific regression coefficients. The covariance matrix  $\boldsymbol{\Sigma}_{\mathbf{Y}}$  describes the residual dependence among the five metabolic components at a given visit. We assign the following marginal prior:

$$\boldsymbol{\Sigma}_{\mathbf{Y}} \sim IW(\nu_{\mathbf{Y}}, \boldsymbol{\Psi}_{\mathbf{Y}}), \quad (3)$$

where  $IW(\nu, \boldsymbol{\Psi})$  denotes the Inverse-Wishart distribution with  $\nu$  degrees of freedom and scale

matrix  $\Psi$ , such that  $E(\Sigma_Y) = \frac{\Psi_Y}{\nu - K - 1}$ .

Regarding the regression matrix  $\beta$ , to perform structured variable selection while encouraging joint sparsity across outcomes, we assign a horseshoe prior to  $\beta$ . Covariates are partitioned into three groups  $C \in \{\text{Numerical, Binary, Interactions}\}$ . Thus, for each covariate index  $p = 1, \dots, P$  belonging to group  $C$  and each outcome  $k = 1, \dots, K$ , we define

$$\beta_{pk} = \tau_C \lambda_p z_{pk} \quad \text{for all } p \text{ associated to covariate of type } C, \quad (4)$$

where  $\{z_{pk}\}$ ,  $\{\lambda_p\}$ ,  $\{\tau_C\}$  are independent with

$$z_{pk} \stackrel{\text{iid}}{\sim} \mathcal{N}(0, 1), \quad \lambda_p \stackrel{\text{iid}}{\sim} \text{Cauchy}^+(0, 1), \quad \tau_C \stackrel{\text{iid}}{\sim} \text{Cauchy}^+(0, 1). \quad (5)$$

Here,  $\lambda_p$  is a covariate-specific local scale parameter shared across all  $K$  outcomes, while  $\tau_C$  is a group-specific global shrinkage parameter shared across all covariates of type  $C$  and across outcomes. Hence, the regression coefficients are conditionally independent given their respective global and local scale parameters. This shared global–local structure induces joint shrinkage of the coefficients associated with a given covariate across the five targets, favoring predictors that are informative for multiple MetS components. A coefficient  $\beta_{pk}$  can escape substantial shrinkage only if the corresponding  $\lambda_p$  is sufficiently large, thereby promoting parsimonious yet jointly predictive multivariate models.

We assume the donor-specific random intercepts  $\mathbf{b}_i$  to be exchangeable and model them with the following multivariate hierarchical prior:

$$\mathbf{b}_i \mid \boldsymbol{\mu}_b, \boldsymbol{\Sigma}_b \stackrel{\text{iid}}{\sim} \mathcal{N}_K(\boldsymbol{\mu}_b, \boldsymbol{\Sigma}_b), \quad i = 1, \dots, I, \quad \boldsymbol{\mu}_b \sim \mathcal{N}_K(\mathbf{0}, \mathbf{I}_K), \quad \boldsymbol{\Sigma}_b \sim IW(\nu_b, \Psi_b). \quad (6)$$

The matrix  $\boldsymbol{\Sigma}_b$  captures the correlation among donor-specific random intercepts across the five outcomes. Formulation (1)-(6) defines a multivariate regression model with outcome-specific coefficient vectors, coupled through shared shrinkage and covariance structures.

We conclude the model specification by discussing temporal dependence and the handling of missing outcome values. We examine whether the model specification can be improved by incorporating a Continuous Autoregressive (t-CAR) structure to account for unequally spaced visits. As detailed in Appendices B.1 and B.2, we assess this autoregressive component in both the joint multivariate and independent univariate settings. In all cases, posterior estimates of the t-CAR decay parameters indicate that temporal autocorrelation drops to virtually zero over the

typical time intervals between consecutive blood donations. Furthermore, model comparison based on WAIC and LOOIC (Appendix B.3) confirms that adding t-CAR terms yields no out-of-sample predictive gain over the likelihood specification (1)-(2). This predictive evaluation also supports the superiority of the joint multivariate framework over independent models. By borrowing strength across correlated metabolic targets, the multivariate structure reduces uncertainty in imputing missing outcome values. Given these results and the fact that age interactions already partially capture longitudinal metabolic dynamics, no autoregressive components are included in the final model to preserve parsimony and maintain computational efficiency.

For observations with missing *waist circumference*, the corresponding log-scaled measurement  $Y_{ij}^{(k)}$ —where  $k = \textit{waist circumference}$ —is treated as an unknown parameter and is estimated jointly with the other model parameters via data augmentation. Details are provided in Appendix A.3.

Under the final model specification described by (1)-(6), inference relies on the posterior distribution of all unknown parameters obtained via MCMC sampling.

## 4 Traffic-light warning system

To translate the probabilistic outputs of the Bayesian multivariate model (1)-(6) into actionable clinical information, we develop a traffic-light warning system that stratifies donors into three risk levels: low (green), potential (yellow), and high (red) risk of MetS. The classification depends not only on the estimated posterior predictive probability that a donor meets the diagnostic criteria for MetS at a *future* visit, but also accounts for the uncertainty around this estimate. For each donor  $i$  at visit  $n_i + 1$ , for  $i = 1, \dots, I$  in the testing set, let  $S_{i, n_i+1}$  denote the indicator that the donor satisfies the MetS diagnostic criteria at visit  $n_i + 1$ . Given the available covariate vector  $\mathbf{x}_{i, n_i+1}$ , our goal is to estimate the posterior predictive probability  $P(S_{i, n_i+1} = 1 \mid \text{data}, \mathbf{x}_{i, n_i+1})$ . This quantity is approximated via MCMC. At each posterior draw of the model parameters, we simulate the future outcomes  $\mathbf{Y}_{i, n_i+1}$  according to the likelihood (1)-(2), and we set  $S_{i, n_i+1} = 1$  if and only if at least three out of the five components meet the thresholds in Table 1. The average of the resulting MCMC samples provides an estimate of the posterior predictive probability that donor  $i$  will have MetS at visit  $n_i + 1$ . For 710 donors, the observed outcome  $s_{i, n_i+1}$  is also available, and it will be used to assess the traffic-light classification in Section 6. In addition to the posterior mean, we compute the 2.5th and 97.5th percentiles of the MCMC samples, thus obtaining a 95% credible interval for the posterior predictive probability. Since the prevalence of MetS is very low in this healthy population, the traffic-light classification is based not solely on the posterior mean but also on its posterior uncertainty.

Donors are assigned to risk categories by comparing the posterior mean and the 95% credible interval of the posterior predictive distribution of  $S_{i_{n_i+1}} = 1$ , given the available covariates, against a fixed probability threshold  $t$ . The threshold  $t$  is selected from a grid of candidate values using the ROC curve, choosing the value that maximizes Youden’s  $J$  statistic ( $J = \text{sensitivity} + \text{specificity} - 1$ ). This criterion achieves the best balance between sensitivity and specificity. Arbitrary thresholds (e.g., 50% or empirical prevalence) lead to suboptimal classification: in low-prevalence settings, a 50% cutoff increases false negatives, while using the empirical prevalence overly favors sensitivity at the expense of specificity. Ultimately, we classify donor  $i$  at visit  $n_i + 1$  in the following categories:

- **Green** (low risk): when both the posterior mean and the upper bound of the credible interval fall below the threshold  $t$ , indicating a very low risk;
- **Yellow** (potential risk): when the posterior mean is below the threshold  $t$ , but the upper bound exceeds it, indicating uncertainty with potential elevated risk;
- **Red** (high risk): when the posterior mean of the credible interval exceeds the threshold  $t$ , consistent with strong evidence of MetS.

In this preventive screening setting, sensitivity is prioritized over specificity, since failing to identify donors who may meet the MetS criteria would be clinically more consequential than assigning additional donors to closer monitoring. This traffic-light algorithm also helps identify false negatives, which we expect in this low-prevalence setting, where it is challenging for a classification model to distinguish donors with and without MetS. The yellow light provides an additional warning signal, thereby boosting the model’s sensitivity. In this way, the model yields an ordered classification of risk, helping clinicians identify donors who may require closer monitoring during clinical checkups.

## 5 Posterior inference

We compute the posterior distribution of the Bayesian model (1)-(6) using an MCMC algorithm based on the training set. In particular, we employ Hamiltonian Monte Carlo through the software platform Stan (Carpenter et al., 2017). We fix moderately informative hyperparameters,  $\nu_Y = \nu_b = 10$ ,  $\Psi_Y = 2I$ , and  $\Psi_b = 12I$ , so that  $E(\Sigma_Y) = 0.5I$  and  $E(\Sigma_b) = 3I$ . Under this specification, the prior variances are  $\text{Var}(\Sigma_{Y,ii}) = 0.25$  and  $\text{Var}(\Sigma_{b,ii}) = 9$  for the diagonal elements, and  $\text{Var}(\Sigma_{Y,ij}) \approx 0.167$  and  $\text{Var}(\Sigma_{b,ij}) = 6$  for the off-diagonal elements ( $i \neq j$ ). Since the target variables are standardized before modeling, this prior maintains a relatively small expected residual variance for within-donor fluctuations ( $\Sigma_Y$ ), while acting as a permissive, weakly informative prior for the random effects ( $\Sigma_b$ ), allowing the model to capture substantial baseline heterogeneity across

donors freely. We run four parallel MCMC chains with 1,000 burn-in and 1,000 sampling iterations each, for a total of 4,000 draws. Convergence of the MCMC algorithm has been assessed: no divergent transitions were reported during sampling and the E-BFMI diagnostic metric indicates no pathological behavior in the energy exploration. We have also performed a sensitivity analysis on the prior hyperparameters of the random-effects covariance matrix, namely  $\Psi_b$  and  $\nu_b$ , and obtained consistent posterior results across different prior specifications.

Our Bayesian hierarchical multivariate mixed-effects model provides robust and interpretable inferences on individual MetS risk within the AVIS Milan donor population. Table 4 shows that only a small subset of predictors remains clearly associated with the MetS component variables, while most coefficients are shrunk toward zero by the horseshoe prior. The posterior means of the fixed effects are consistent with established clinical knowledge: *BMI*, *age*, and *sex* emerge as central determinants across the five MetS biomarker outcomes. Not surprisingly, *BMI* shows strong positive associations with *PMAX*, *triglycerides*, *waist circumference*, and *glucose*, and a strong negative association with *HDL cholesterol*. Male *sex* is negatively correlated with *HDL cholesterol*, confirming that men physiologically tend to have lower *HDL cholesterol* levels, and positively correlated with all the other target variables. These findings are consistent with known *sex* differences in lipid metabolism and blood pressure regulation (Regitz-Zagrosek et al., 2016). The *age* is one of the main drivers of all five target variables. Moreover, the interaction between *age* and *sex* appears predictive for *PMAX*, *glucose*, and *waist circumference*. This supports the evidence that metabolic risk trajectories are gender-dependent, often showing different slopes of progression as individuals age, particularly during hormonal shifts in women (Regitz-Zagrosek et al., 2016).

The presence of non-zero coefficients for *HDL cholesterol* associated with the two red blood cell indices, *MCH* and *MCHC*, which are related to hemoglobin content and concentration, suggests that these indices may capture additional information about lipid metabolism beyond traditional MetS markers. Higher or lower *MCH/MCHC* values often reflect subtle alterations in iron status, chronic inflammation, or nutritional deficiencies, all of which have been associated with atherogenic dyslipidemia and variations in *HDL* levels (Weiss et al., 2019; Krawiec and Pac-Kożuchowska, 2020; Clucas and Biggs, 2022). Their significance in our model supports the notion that low-grade inflammatory or hematologic changes may coexist with the dyslipidemic profile typical of MetS.

Finally, most interaction terms between *sex* and other covariates are not statistically relevant. Notably, only the *BMI*  $\times$  *sex* interaction shows relevance, with negative coefficients for *HDL cholesterol* and *waist circumference*, indicating that the effect of *BMI* on *waist circumference* is stronger in women than in men. In contrast, the negative association of *age* with *HDL cholesterol*

Covariate	glucose	HDL	PMAX	triglycerides	waist circumference
ALT	0.01 (-0.01, 0.04)	0.01 (-0.01, 0.02)	-0.01 (-0.03, 0.01)	0.02 (-0.00, 0.04)	0.01 (-0.01, 0.02)
Age	0.11 (0.04, 0.16)	0.05 (0.01, 0.10)	0.29 (0.22, 0.34)	0.17 (0.12, 0.23)	0.19 (0.13, 0.22)
BMI	0.05 (-0.01, 0.11)	-0.17 (-0.23, -0.11)	0.19 (0.13, 0.25)	0.17 (0.10, 0.23)	0.64 (0.60, 0.68)
Basophils_pct	-0.01 (-0.03, 0.01)	0.02 (0.01, 0.04)	0.01 (-0.01, 0.03)	-0.01 (-0.03, 0.01)	-0.01 (-0.02, 0.00)
Creatinine	-0.01 (-0.03, 0.01)	-0.01 (-0.03, 0.01)	-0.02 (-0.04, 0.00)	0.02 (0.01, 0.05)	-0.02 (-0.04, -0.01)
Eosinophils_pct	-0.00 (-0.02, 0.02)	-0.04 (-0.05, -0.02)	-0.01 (-0.03, 0.01)	0.06 (0.04, 0.08)	-0.00 (-0.01, 0.01)
Ferritin	0.00 (-0.02, 0.02)	-0.03 (-0.05, -0.01)	0.01 (-0.01, 0.03)	-0.01 (-0.03, 0.01)	0.01 (-0.01, 0.02)
Heart_rate	0.01 (-0.02, 0.04)	-0.01 (-0.03, 0.01)	0.08 (0.02, 0.11)	0.03 (0.00, 0.06)	0.00 (-0.02, 0.02)
Height	-0.00 (-0.05, 0.04)	-0.02 (-0.07, 0.03)	0.01 (-0.03, 0.06)	-0.01 (-0.06, 0.04)	0.23 (0.19, 0.26)
Hemoglobin	0.01 (-0.04, 0.05)	0.10 (0.06, 0.13)	0.07 (0.02, 0.11)	0.11 (0.05, 0.16)	0.01 (-0.03, 0.03)
Lymphocytes_pct	-0.02 (-0.05, 0.01)	-0.01 (-0.03, 0.01)	-0.03 (-0.06, -0.00)	0.04 (0.01, 0.07)	-0.01 (-0.03, 0.01)
MCH	0.02 (-0.03, 0.06)	0.10 (0.06, 0.14)	-0.08 (-0.12, -0.04)	-0.03 (-0.07, 0.01)	-0.03 (-0.05, 0.01)
MCHC	-0.09 (-0.12, -0.06)	-0.09 (-0.10, -0.07)	0.03 (-0.00, 0.05)	0.02 (-0.00, 0.04)	0.00 (-0.01, 0.02)
Monocytes_pct	-0.09 (-0.11, -0.07)	-0.01 (-0.02, 0.01)	-0.04 (-0.06, -0.02)	-0.03 (-0.04, -0.01)	0.01 (-0.01, 0.02)
Platelets	-0.00 (-0.02, 0.02)	0.01 (-0.00, 0.04)	-0.00 (-0.02, 0.02)	0.01 (-0.01, 0.03)	0.00 (-0.01, 0.02)
Total_proteins	0.01 (-0.01, 0.03)	0.03 (0.02, 0.04)	0.00 (-0.02, 0.02)	0.02 (0.00, 0.03)	-0.00 (-0.01, 0.01)
Volume_distribution	0.00 (-0.03, 0.04)	0.03 (-0.00, 0.08)	0.01 (-0.03, 0.04)	-0.02 (-0.06, 0.01)	-0.00 (-0.03, 0.02)
WBC	-0.00 (-0.05, 0.05)	0.01 (-0.02, 0.05)	-0.03 (-0.07, 0.01)	0.09 (0.03, 0.15)	0.00 (-0.03, 0.03)
Physical_activity_Active	-0.02 (-0.06, 0.02)	-0.01 (-0.04, 0.02)	0.00 (-0.05, 0.03)	0.00 (-0.03, 0.03)	-0.04 (-0.09, 0.01)
sex_Male	0.15 (0.02, 0.28)	-0.94 (-1.08, -0.80)	0.25 (0.13, 0.38)	0.19 (0.05, 0.34)	0.33 (0.24, 0.43)
ALT × sex	0.00 (-0.01, 0.03)	0.00 (-0.01, 0.02)	0.00 (-0.01, 0.02)	0.01 (-0.01, 0.04)	0.00 (-0.01, 0.01)
Age × sex	0.02 (-0.02, 0.10)	0.01 (-0.04, 0.07)	0.03 (-0.01, 0.11)	-0.00 (-0.06, 0.04)	0.03 (-0.01, 0.08)
BMI × sex	0.05 (-0.01, 0.11)	-0.11 (-0.18, -0.05)	0.03 (-0.03, 0.10)	0.06 (-0.01, 0.13)	-0.06 (-0.10, -0.02)
Creatinine × sex	-0.00 (-0.02, 0.01)	-0.00 (-0.01, 0.01)	-0.00 (-0.02, 0.01)	-0.00 (-0.02, 0.01)	0.00 (-0.01, 0.02)
Ferritin × sex	-0.00 (-0.02, 0.02)	-0.00 (-0.02, 0.01)	0.00 (-0.01, 0.03)	-0.00 (-0.02, 0.01)	-0.00 (-0.02, 0.01)
Hemoglobin × sex	0.00 (-0.04, 0.04)	0.01 (-0.01, 0.05)	0.00 (-0.04, 0.05)	0.03 (-0.01, 0.10)	0.01 (-0.02, 0.04)
Heart_rate × sex	0.01 (-0.01, 0.05)	-0.00 (-0.02, 0.01)	0.02 (-0.01, 0.08)	0.01 (-0.01, 0.05)	0.01 (-0.01, 0.03)
Height × sex	-0.00 (-0.03, 0.04)	-0.01 (-0.06, 0.02)	-0.00 (-0.04, 0.03)	-0.00 (-0.05, 0.02)	0.00 (-0.03, 0.04)
Lymphocytes_pct × sex	-0.00 (-0.03, 0.01)	-0.00 (-0.02, 0.02)	-0.00 (-0.03, 0.01)	0.00 (-0.02, 0.03)	0.00 (-0.01, 0.02)
MCH × sex	0.01 (-0.02, 0.06)	0.01 (-0.02, 0.06)	-0.00 (-0.04, 0.03)	-0.01 (-0.06, 0.02)	-0.02 (-0.06, 0.00)
PhAct × sex	-0.01 (-0.05, 0.03)	0.00 (-0.02, 0.03)	0.01 (-0.02, 0.06)	0.00 (-0.03, 0.04)	-0.03 (-0.10, 0.01)
Platelets × sex	0.00 (-0.02, 0.02)	0.01 (-0.01, 0.03)	0.00 (-0.01, 0.02)	0.00 (-0.02, 0.02)	0.00 (-0.01, 0.02)
Volume × sex	-0.02 (-0.06, 0.01)	0.05 (0.00, 0.09)	0.01 (-0.02, 0.05)	0.00 (-0.03, 0.04)	-0.00 (-0.03, 0.02)
WBC × sex	-0.03 (-0.09, 0.01)	-0.03 (-0.07, 0.00)	0.00 (-0.03, 0.05)	0.05 (-0.00, 0.11)	0.01 (-0.01, 0.04)

Table 4: Posterior means and 95% credible intervals of the fixed effects for each covariate across the five target variables. Green and red colors denote positive and negative coefficients whose 95% credible intervals exclude zero, respectively.

appears more pronounced in men.

Our hierarchical Bayesian model explicitly accounts for correlations among the five target variables by modeling a full covariance structure for both the random intercepts ( $\Sigma_b$ ) and the residuals ( $\Sigma_Y$ ). Figure 1 shows the posterior means of the correlation matrices  $\Sigma_Y$  and  $\Sigma_b$ , revealing

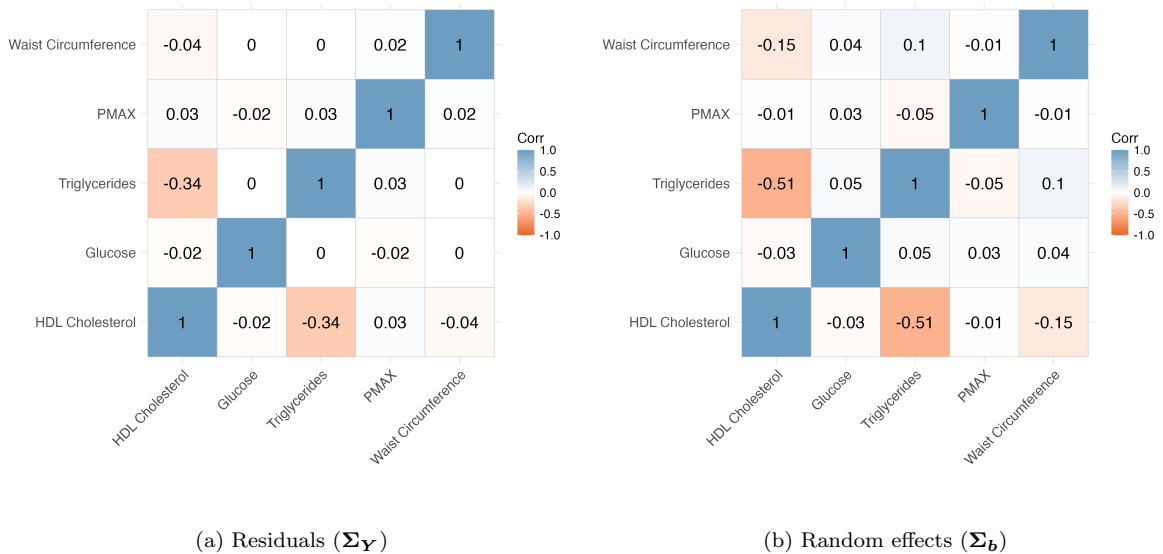


Figure 1: Posterior mean correlation matrices of the residuals ( $\Sigma_Y$ ) and random effects ( $\Sigma_b$ ).

predominantly weak correlations. The strongest residual correlation is observed between *HDL cholesterol* and *triglycerides* ( $-0.34$ ) (Figure 1, panel a). Panel (b) shows stronger correlations at the random intercept level, including *triglycerides-HDL-cholesterol* ( $-0.52$ ), *waist circumference-HDL-cholesterol* ( $-0.15$ ), and *waist circumference-triglycerides* ( $0.11$ ).

These results offer important insights into pathophysiology and modeling. The moderate negative correlation between *HDL cholesterol* and *triglycerides*, present both at the residual and subject-specific level, reflects the well-documented biological inverse relationship between these two lipids, a hallmark of atherogenic dyslipidemia and insulin resistance (Rashid et al., 2003). Crucially, the stronger correlations in the random intercepts ( $\Sigma_b$ ) than in the residuals ( $\Sigma_Y$ ) indicate that the underlying metabolic dependence is primarily driven by unobserved, time-invariant individual characteristics (e.g., genetic predispositions or long-term lifestyle habits not fully captured by covariates) rather than short-term fluctuations. These non-negligible correlations support modeling the dependence structure among target variables rather than treating them as independent.

## 6 Evaluation of the traffic-light warning system

Our primary clinical objective is to classify test set donors using the traffic-light warning system detailed in Section 4. The classification relies on the optimal threshold  $t = 0.099$ , obtained by maximizing Youden’s  $J$  statistic on the training set. It is important to note that classification performance is evaluated against a ground truth available only for the 710 test set donors with complete target variable measurements.

The first row of Table 5 reports the confusion matrix and the classification metrics from the traffic-light algorithm. To compute standard binary metrics – namely sensitivity (true positive rate: correctly identified MetS cases), specificity (true negative rate: correctly identified non-MetS cases), and accuracy (overall correct classification rate) – for this three-tier system, we dichotomize our prediction: we consider both the yellow and red categories as a positive MetS prediction (indicating potential or high risk requiring attention), and the green category as a negative prediction. Under this stratification, the algorithm directly recovers 61 true MetS cases (red category) and classifies the remaining 5 affected donors as yellow. Consequently, the traffic-light algorithm achieves a sensitivity of 100%, ensuring that all donors with the syndrome are effectively captured and assigned to the yellow or red risk categories. Approximately 38% of observations are flagged as medium- or high-risk, compared with an overall syndrome prevalence of 9.3% in the test set. This *conservative* approach perfectly aligns with the goals of a preventive screening setting: it minimizes false negatives at the cost of a low specificity (67.9%) and an overall

Model		Confusion Matrix		Performance Metrics		
		True No	True Yes	Sens	Spec	Acc
Traffic-light algorithm	Green	437	0	100%	67.9%	70.8%
	Yellow	112	5			
	Red	95	61			
Direct Bayesian binary	Pred No	549	5	92.4%	85.2%	85.9%
	Pred Yes	95	61			
LGBM	Pred No	500	16	75.8%	77.6%	77.5%
	Pred Yes	140	50			
LR	Pred No	369	6	90.9%	57.3%	60.4%
	Pred Yes	275	60			
LDA	Pred No	390	6	90.9%	60.5%	63.4%
	Pred Yes	254	60			
KNN	Pred No	453	19	71.2%	70.3%	70.4%
	Pred Yes	191	47			

Table 5: Confusion matrix (second column) and performance metrics (third column) of the test set donors under different models/classifiers (listed in the first column). The confusion matrix in all the rows, but the second, concerns a binary classification (No/Yes = MetS Negative/Positive). For the traffic-light algorithm, Green is treated as Pred No, while the Yellow and Red are treated as Pred Yes.

accuracy of only 70.8%.

To evaluate the absolute discriminative performance of the Bayesian model, we also consider the associated direct binary classification. In this strict setting, donors with a predicted probability strictly below  $t = 0.099$  are classified as MetS negative, whereas those at or above the threshold are classified as MetS positive. The second row of Table 5 details the confusion matrix and the performance metrics for this binary formulation. The direct classification demonstrates strong predictive power, correctly identifying 92.4% of at-risk donors while maintaining a high specificity (85.2%) and accuracy (85.9%). This confirms that the underlying multivariate framework robustly discriminates between affected and healthy profiles, even before the prudential yellow-light zone is introduced.

We further assess the robustness of our model through a simulation study that replicates the longitudinal structure of the AVIS Milan cohort while accounting for model misspecification and temporal dependence. Specifically, we simulated data with an autoregressive dynamics and heavy-tailed noise that are not explicitly accounted for in the likelihood in (1)-(2). Despite these departures from the model assumptions, our model still yields accurate out-of-sample predictions. Full details on the simulation design and posterior predictive evaluation are provided in Appendix C.

## 7 Comparison with alternative classification methods

We compare the results described in Section 6 with several widely used classification approaches, including Light Gradient Boosting Machine (Ke et al., 2017, LGBM), Logistic Regression (LR), Linear Discriminant Analysis (LDA), and K-Nearest Neighbors (KNN). LR, LDA, and KNN are standard statistical techniques in biomedical research, providing transparent parametric (LR, LDA) or distance-based (KNN) decision rules with coefficients or decision boundaries that can be readily interpreted clinically. In contrast, LGBM is a modern ML method based on gradient-boosted decision trees, designed to maximize predictive accuracy on tabular data by enabling flexible nonlinear interactions and automatically handling complex feature relationships, albeit at the cost of reduced interpretability.

We fit LR, LDA, KNN, and LGBM in R using the training set restricted to complete observations. Cases with missing *waist circumference* are excluded, as these models cannot automatically impute partial missing values in the response. The alternative models are trained using the same covariates as in our Bayesian model (as in (2)) and are reported in Table 2. We fit LGBM via the R package `lightgbm` v4.6.0 (Shi et al., 2025). The hyperparameters are tuned via Bayesian optimization using the `rBayesianOptimization` package (Yan, 2025). LR is fitted using the `glmnet` (Friedman et al., 2010) package in R. We set  $\alpha = 1$  to impose a LASSO penalty on the coefficients, and the optimal regularization strength  $\lambda$  is selected via 5-fold cross-validation. KNN is trained using the `class` package, with the optimal number of neighbors  $k$  selected via leave-one-out cross-validation. LDA is fitted using the `MASS` package in R, requiring no hyperparameter tuning. All these models output class probabilities that require a classification threshold. For each method, we select the threshold  $t$  that maximizes the associated Youden’s  $J$  statistic, obtaining  $t = 0.067$  for LDA,  $t = 0.066$  for LR,  $t = 0.090$  for KNN, and  $t = 0.747$  for LGBM. These thresholds yield the final hard predictions for each observation.

Table 5 shows that the traffic-light algorithm achieves perfect sensitivity, successfully identifying all 66 true MetS cases in yellow or red categories. The direct Bayesian binary classification also delivers strong performance (92.4% sensitivity, 85.2% specificity, 85.9% accuracy). By comparison, LGBM misses 16 cases, KNN misses 19, while LR and LDA (90.9% sensitivity) show lower specificity (57-60%) than the traffic-light algorithm’s 67.9%.

A key advantage of our approach lies in its generative hierarchical formulation. Our Bayesian model specifies the joint distribution of the five MetS biomarkers conditional on covariates, explicitly modeling longitudinal dependence and cross-outcome correlations. Classification is then derived as a secondary step from the posterior predictive distribution. In contrast, LR, LDA,

KNN, and LGBM are purely discriminative classifiers that directly approximate the conditional probability of class membership without modeling the underlying multivariate structure of the biomarkers. On the other hand, a notable advantage of LGBM, LR, KNN, and LDA models is their low computational cost: model fitting required only a few minutes, whereas running the MCMC for our model took approximately three hours on a MacBook Pro with an M4 Pro chip and 24GB of RAM.

## 8 Discussion

This study focuses on predicting MetS risk at future check-ups by proposing and validating a Bayesian multivariate mixed-effects model for longitudinal clinical and lifestyle data collected from mostly healthy blood donors. Unlike most existing approaches, which rely on cross-sectional or clinically compromised cohorts, our analysis leverages repeated measurements from healthy donors to capture the temporal evolution and interdependence of metabolic risk factors before disease onset. Including subject-specific random effects further enhances the model’s ability to account for unobserved heterogeneity.

Although blood donors are generally healthy, they exhibit substantial variability in lifestyle, genetic predisposition, and long-term health trajectories. By capturing individual baseline differences and within-subject temporal correlations, the model yields personalized risk estimates that extend beyond population-level averages, aligning with the principles of precision medicine. The horseshoe prior enables automatic variable selection, improving the interpretability of the key drivers of MetS components while preventing overfitting. The model simultaneously imputes missing outcomes and performs inference, estimating MetS risk through posterior predictive samples by evaluating whether at least three clinical thresholds are met. Rather than relying on binary classification, a three-level traffic-light system (low, intermediate, high risk) supports early identification and targeted interventions. This approach achieves high sensitivity while reducing unnecessary follow-ups and prioritizing high-risk individuals.

From a practical perspective, the method enables large-scale, low-cost screening of healthy individuals. In particular, the derived risk score allows AVIS Milan clinicians to allocate time and resources more efficiently by focusing on high-risk subjects, while limiting unnecessary visits and diagnostic procedures for those at low risk. This is especially relevant in the context of blood donation, where regular monitoring offers an opportunity for timely lifestyle interventions to preserve donor health. Maintaining donor health also supports continuity in blood donation and contributes to a stable blood supply for healthcare systems.

The algorithm will be integrated into the AVIS Milan clinical decision support system soon, with its effectiveness supported by feedback from medical staff. Translating probabilistic outputs into an intuitive traffic-light classification represents a key step toward clinical applicability, facilitating decision-making during routine screening. In settings with limited time and resources, such as blood donation centers, this framework enhances efficiency by prioritizing individuals who may benefit from further evaluation. The high sensitivity of the system (Table 5) ensures that most at-risk individuals are identified, while the stratification into ordered risk categories reduces unnecessary follow-ups and supports clinical prioritization.

Beyond risk stratification, the model identifies the key drivers among MetS components, highlighting the covariates that most strongly influence each outcome. At the same time, our findings emphasize that metabolic risk factors are not uncommon even in populations considered healthy. The longitudinal nature of the AVIS Milan dataset offers a unique opportunity to monitor subtle changes in metabolic profiles over time, reinforcing the value of blood donation centers as platforms for large-scale preventive screening.

The large number of donors primarily drives the model’s computational cost, although most contribute only a few repeated measurements (typically 3-5, as shown in Figure A.1). For each donor, the model estimates a  $K$ -dimensional vector of random intercepts, increasing computational complexity. Nevertheless, the model can be fitted in approximately three hours on a standard laptop, making routine retraining feasible as new data become available.

Despite its strengths, several limitations should be acknowledged. First, the model’s generalizability may be limited by the specific characteristics of the AVIS Milan population, including its demographic composition and eligibility criteria. External validation on more diverse populations is therefore necessary. Second, while the traffic-light system improves usability, the choice of risk thresholds involves a trade-off between sensitivity and specificity and may require calibration depending on the clinical context. Finally, although the model relies on routinely collected clinical and lifestyle variables, it may omit relevant factors such as genetic information, detailed dietary patterns, or socioeconomic determinants, whose inclusion could further improve predictive performance.

## Acknowledgments

The authors wish to express their sincere appreciation to AVIS Milan for involving us in their activities, for providing the data, for testing the developed tool, and for the support offered. Special thanks are extended to the Director Sergio Casartelli for the valuable support throughout

the development of this research.

## Funding

The first three authors acknowledge the support of MUR, grant Dipartimento di Eccellenza 2023–2027.

## References

- Air, E. L. and Kissela, B. M. (2007). Diabetes, the metabolic syndrome, and ischemic stroke. *Diabetes Care*, 30(12).
- Alberti, K. G. M. M., Zimmet, P., and Shaw, J. (2006). Metabolic syndrome—a new world-wide definition. A consensus statement from the International Diabetes Federation. *Diabetic Medicine*, 23(5):469–480.
- Ascherio, A., Rimm, E. B., Giovannucci, E., Willett, W. C., and Stampfer, M. J. (2001). Blood donations and risk of coronary heart disease in men. *Circulation*, 103(1):52–57.
- Cai, B. and Dunson, D. B. (2006). Bayesian covariance selection in generalized linear mixed models. *Biometrics*, 62(2):446–457.
- Carpenter, B., Gelman, A., Hoffman, M. D., Lee, D., Goodrich, B., Betancourt, M., Brubaker, M., Guo, J., Li, P., and Riddell, A. (2017). Stan: A probabilistic programming language. *Journal of Statistical Software*, 76(1).
- Clucas, D. and Biggs, B.-A. (2022). Interpretation of biomarkers and diagnosis of nutritional anaemias. In *Nutrition and Health*, pages 49–62. Springer International Publishing, Cham.
- de Bakker, M., Gordon, B., Shah, A., Boersma, E., and Kimenai, D. M. (2025). Circulating cardiovascular biomarkers in motion: redefining cardiovascular risk with dynamic prediction. *European Journal of Preventive Cardiology*, page zwaf76.
- Diggle, P. J. (1988). An approach to the analysis of repeated measurements. *Biometrics*, 44:959–971.
- Dunson, D. B. (2003). Dynamic latent trait models for multidimensional longitudinal data. *Journal of the American Statistical Association*, 98(463):555–563.

- Epifani, I., Lanzarone, E., and Guglielmi, A. (2025). Predicting donations and profiling donors in a blood collection center: a Bayesian approach. *Flexible Services and Manufacturing Journal*, 37(4):1093–1116.
- Friedman, J., Hastie, T., and Tibshirani, R. (2010). Regularization paths for generalized linear models via coordinate descent. *Journal of statistical software*, 33(1):1–22.
- Germain, M., Delage, G., Blais, C., Maunsell, E., Décary, F., and Grégoire, Y. (2013). Iron and cardiac ischemia: a natural, quasi-random experiment comparing eligible with disqualified blood donors. *Transfusion*, 53(6):1271–1279.
- Goldman, O., Ben-Assuli, O., Ababa, S., Rogowski, O., and Berliner, S. (2025). Predicting metabolic syndrome: Machine learning techniques for improved preventive medicine. *Health Informatics Journal*, 31(1):14604582251315602.
- Grundy, S. M., Cleeman, J. I., Daniels, S. R., Donato, K. A., Eckel, R. H., Franklin, B. A., Gordon, D. J., Krauss, R. M., Savage, P. J., Smith Jr, S. C., et al. (2005). Diagnosis and management of the metabolic syndrome: an American Heart Association/National Heart, Lung, and Blood Institute scientific statement. *Circulation*, 112(17):2735–2752.
- Han, Y., Albert, P. S., Berg, C. D., Wentzensen, N., Katki, H. A., and Liu, D. (2020). Statistical approaches using longitudinal biomarkers for disease early detection: A comparison of methodologies. *Statistics in Medicine*, 39(29):4405–4420.
- International Diabetes Federation (2025). *IDF Diabetes Atlas*. International Diabetes Federation, Brussels, Belgium.
- Isomaa, B., Almgren, P., Tuomi, T., Forsen, B., Lahti, K., Nissen, M., Taskinen, M.-R., and Groop, L. (2001). Cardiovascular morbidity and mortality associated with the metabolic syndrome. *Diabetes care*, 24(4):683–689.
- Kassi, E., Pervanidou, P., Kaltsas, G., and Chrousos, G. (2011). Metabolic syndrome: definitions and controversies. *BMC medicine*, 9(1):48.
- Ke, G., Meng, Q., Finley, T. R., Wang, T., Chen, W., Ma, W., Ye, Q., and Liu, T.-Y. (2017). LightGBM: A highly efficient gradient boosting decision tree. *Advances in Neural Information Processing Systems*, 30.
- Kim, J., Mun, S., Lee, S., Jeong, K., and Baek, Y. (2022). Prediction of metabolic and pre-metabolic syndromes using machine learning models with anthropometric, lifestyle, and biochemical factors from a middle-aged population in Korea. *BMC Public Health*, 22(1):664.

- Krawiec, P. and Pac-Kozuchowska, E. (2020). Biomarkers and hematological indices in the diagnosis of iron deficiency in children with inflammatory bowel disease. *Nutrients*, 12(5):1358.
- Lee, M., Park, T., Shin, J. Y., and Park, M. (2024). A comprehensive multi-task deep learning approach for predicting metabolic syndrome with genetic, nutritional, and clinical data. *Scientific Reports*, 14:17851.
- Najarian, R. M., Sullivan, L. M., Kannel, W. B., Wilson, P. W., D’Agostino, R. B., and Wolf, P. A. (2006). Metabolic syndrome compared with type 2 diabetes mellitus as a risk factor for stroke: the Framingham Offspring Study. *Archives of Internal Medicine*, 166(1):106–111.
- Noubiap, J. J., Nansseu, J. R., Lontchi-Yimagou, E., Nkeck, J. R., Nyaga, U. F., Ngou, A. T., Tounouga, D. N., Tianyi, F.-L., Foka, A. J., Ndoadoumgue, A. L., et al. (2022). Geographic distribution of metabolic syndrome and its components in the general adult population: a meta-analysis of global data from 28 million individuals. *Diabetes Research and Clinical Practice*, 188:109924.
- Park, J.-E., Mun, S., and Lee, S. (2021). Metabolic syndrome prediction models using machine learning and Sasang constitution type. *Evidence-Based Complementary and Alternative Medicine*, 2021:8315047.
- Peffer, K., Verbeek, A., Swinkels, D., Geurts-Moespot, A., den Heijer, M., and Atsma, F. (2015). Donation intensity and metabolic syndrome in active whole-blood donors. *Vox Sanguinis*, 109(1):25–34.
- Quee, F. A., Peffer, K., Ter Braake, A. D., and Van den Hurk, K. (2022). Cardiovascular benefits for blood donors? A systematic review. *Transfusion Medicine Reviews*, 36(3):143–151.
- Rashid, S., Watanabe, T., Sakaue, T., and Lewis, G. F. (2003). Mechanisms of HDL lowering in insulin resistant, hypertriglyceridemic states: the combined effect of HDL triglyceride enrichment and elevated hepatic lipase activity. *Clinical biochemistry*, 36(6):421–429.
- Regitz-Zagrosek, V. et al. (2016). Gender in cardiovascular disease: impact on clinical manifestations, management, and outcomes. *European Heart Journal*, 37(1):24–34.
- Rizopoulos, D., Hatfield, L. A., Carlin, B. P., and Takkenberg, J. J. (2014). Combining dynamic predictions from joint models for longitudinal and time-to-event data using Bayesian model averaging. *Journal of the American Statistical Association*, 109(508):1385–1397.
- Robitzsch, A., Grund, S., and Henke, T. (2021). *miceadds: Some additional multiple imputation functions, especially for “mice”(3.11-6)*.

- Roer, G. E., Bolstad, I., Abebe, D. S., Aaseth, J., Haugen, M., and Lien, L. (2025). Metabolic syndrome and associated risk factors in Norwegian trauma-exposed inpatients: A cross-sectional comparison with blood donors. *Diabetes, Metabolic Syndrome and Obesity*, 4(Aug):2667–2680.
- Salonen, J. T., Tuomainen, T.-P., Salonen, R., Lakka, T. A., and Nyysönen, K. (1998). Donation of blood is associated with reduced risk of myocardial infarction: the Kuopio Ischaemic Heart Disease Risk Factor Study. *American Journal of Epidemiology*, 148(5):445–451.
- Sghaireen, M. G., Al-Smadi, Y., Al-Qerem, A., Srivastava, K. C., Ganji, K. K., Alam, M. K., Nashwan, S., and Khader, Y. (2022). Machine learning approach for metabolic syndrome diagnosis using explainable data-augmentation-based classification. *Diagnostics*, 12(12):3117.
- Shi, Y., Ke, G., et al. (2025). lightgbm: Light Gradient Boosting Machine R package. R package version 4.6.0.
- Shin, H., Shim, S., and Oh, S. (2023). Machine learning-based predictive model for prevention of metabolic syndrome. *PLoS ONE*, 18(6):e0286635.
- Tavares, L. D., Manoel, A., Donato, T. H. R., Cesena, F., Minanni, C. A., Kashiwagi, N. M., da Silva, L. P., Amaro Jr, E., and Szlejf, C. (2022). Prediction of metabolic syndrome: A machine learning approach to help primary prevention. *Diabetes Research and Clinical Practice*, 191:110047.
- Tayob, N., Lok, A. S., and Feng, Z. (2022). A multivariate parametric empirical Bayes screening approach for early detection of hepatocellular carcinoma using multiple longitudinal biomarkers. *Statistics in Medicine*, 41(13):2338–2353.
- Van Buuren, S. (2012). *Flexible Imputation of Missing Data*. CRC Press, Boca Raton, FL.
- Van Buuren, S. and Groothuis-Oudshoorn, K. (2011). mice: Multivariate imputation by chained equations in R. *Journal of statistical software*, 45:1–67.
- Vehtari, A., Gelman, A., and Gabry, J. (2017). Practical Bayesian model evaluation using leave-one-out cross-validation and WAIC. *Statistics and computing*, 27(5):1413–1432.
- Watanabe, S. (2010). Asymptotic equivalence of Bayes cross validation and widely applicable information criterion in singular learning theory. *Journal of Machine Learning Research*, 11(Dec):3571–3594.
- Weiss, G., Ganz, T., and Goodnough, L. T. (2019). Anemia of inflammation. *Blood*, 133(1):40–50.

- World Obesity Federation (2023). *World Obesity Atlas 2023*. World Obesity Federation, London, UK.
- Xu, J. and Zeger, S. L. (2001). The evaluation of multiple surrogate endpoints. *Biometrics*, 57(1):81–87.
- Yan, Y. (2025). *rBayesianOptimization: Bayesian Optimization of Hyperparameters (R package version 1.2.2)*.
- Yang, H., Yu, B., Ouyang, P., Li, X., Lai, X., Zhang, G., and Zhang, H. (2022). Machine learning-aided risk prediction for metabolic syndrome based on 3 years study. *Scientific Reports*, 12(1):2248.
- Zeger, S. L. and Karim, M. R. (1991). Generalized linear models with random effects: A Gibbs sampling approach. *Journal of the American Statistical Association*, 86(413):79–86.

## Appendix

### A Appendix

#### A.1 Exploratory data analysis

Figure A.1 reports the barplot of the donation counts for all the donors in the dataset. The percentage of missing values for each variable in our dataset is shown in Figure A.2. Variables with more than 50% missingness, as *albumin*, *total iron*, *S\_Alpha\_1\_Globulin*, *S\_Alpha\_2\_Globulin*, *S\_Beta\_1\_Globulin*, *S\_Beta\_2\_Globulin*, and *S\_Gamma\_Globulin*, were excluded from analysis to avoid excessive reliance on imputation.

Among the remaining variables, the response variable *waist circumference* exhibits substantial missingness (48%), primarily because it is measured annually for each donor. This level of incompleteness motivates a modeling strategy based on data augmentation, in which missing waist measurements are treated as latent variables within the Bayesian framework, as detailed in Section 3. In contrast, the other target variables (*triglycerides*, *PMAX*, *glucose*, *HDL cholesterol*)

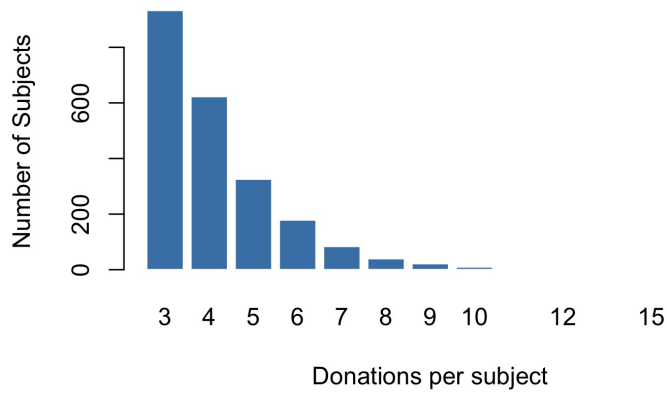


Figure A.1: Barplot of the donation counts for each donor in the dataset.

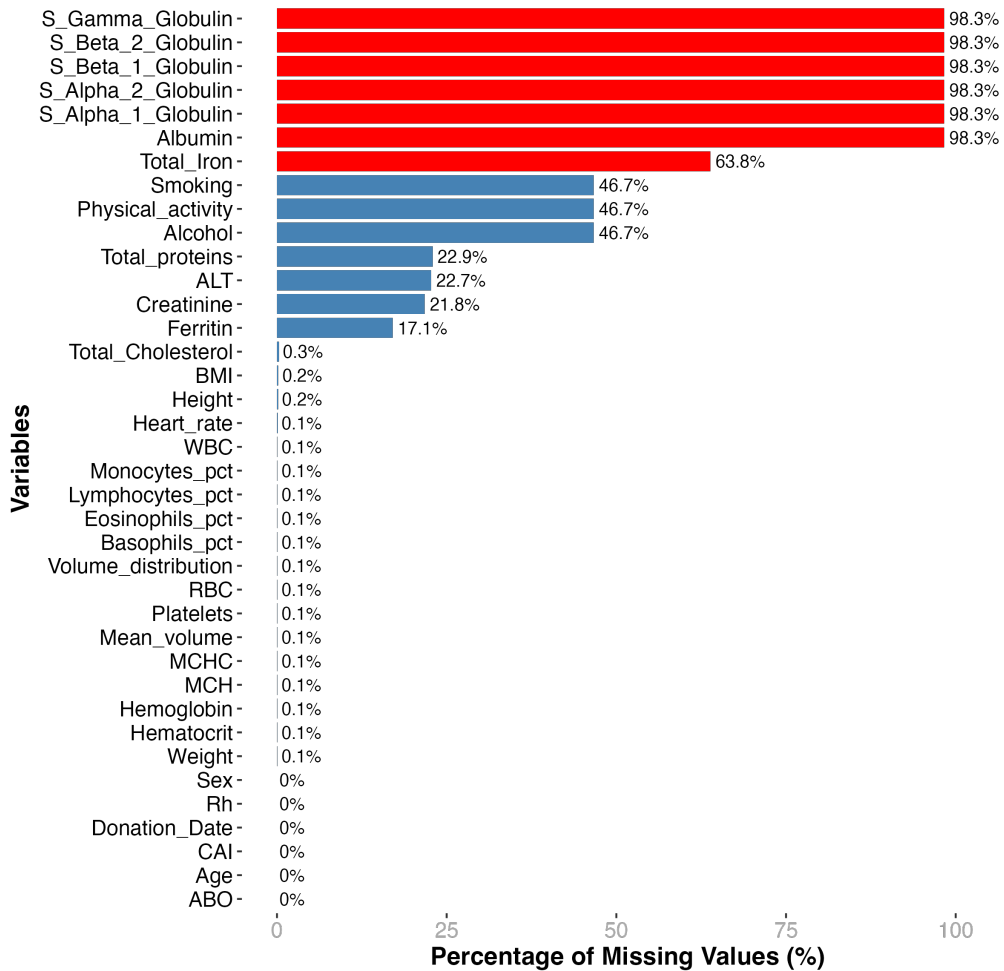


Figure A.2: Percentage of missing values of each covariate. Red bars represent covariates excluded from the analysis, whereas blue bars denote variables handled through imputation.

show very low levels of missingness (below 1%). Questionnaire-derived covariates (*alcohol*, *smoking*, *physical activity*) exhibit 46–47% of observations missing, reflecting the incomplete availability of self-reported information.

Examining the shapes of the distributions of the variables in our dataset, we detect right-skewness across the five target variables and covariates *alanine aminotransferase (ALT)* and *ferritin*, as shown in Figure A.3. Strong right-skewness is evident for *ALT*, *ferritin*, and *triglycerides*, with milder asymmetry observed for *waist circumference*, *glucose*, *PMAX*, and *HDL cholesterol*. This skewness justifies applying log-transformations to these variables to achieve approximately symmetric distributions. We then compute correlations among the numerical covariates in the

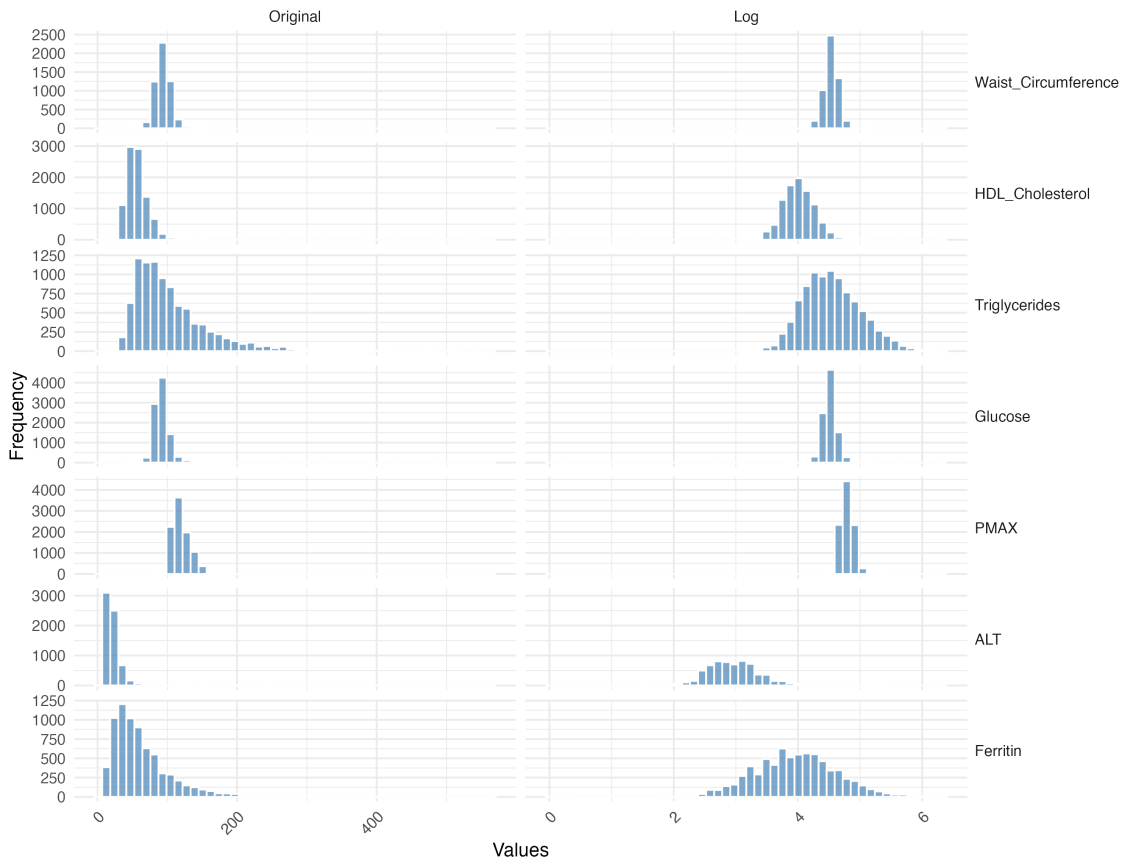


Figure A.3: Histograms of the five target variables and covariates *ALT* and *ferritin*. For each variable, the histogram is shown on the original scale (left) and on the log scale (right).

training set to assess potential multicollinearity. Table A.1 shows the top 20 couples of covariates with the highest correlation in absolute value. Several pairs exhibit high correlations: *hematocrit* with *hemoglobin* ( $r = 0.892$ ), *MCH* with *mean volume (MCV)* ( $r = 0.844$ ), *BMI* with *weight* ( $r = 0.826$ ), and *hematocrit* with *red blood cell count (RBC)* ( $r = 0.799$ ). To improve model interpretability and reduce multicollinearity, we retain *hemoglobin* due to its central physiologi-

cal importance and removed *hematocrit*, *MCV*, *weight*, and *RBC*. Additionally, we exclude *total*

Variable 1	Variable 2	Pearson $r$
Hematocrit	Hemoglobin	0.892
MCH	Mean_volume	0.844
BMI	Weight	0.826
Hematocrit	RBC	0.799
Hemoglobin	RBC	0.697
MCV	RBC	-0.621
MCH	MCHC	0.568
MCH	RBC	-0.567
Height	Weight	0.565
MCH	Volume_distribution	-0.459
MCHC	Volume_distribution	-0.440
Age	CAI	-0.395
Hemoglobin	MCHC	0.366
Creatinine	Hemoglobin	0.339
Creatinine	Height	0.333
Lymphocytes_pct	WBC	-0.315
Basophils_pct	Eosinophils_pct	0.309
Hemoglobin	Weight	0.306
Platelets	WBC	0.295
Height	Hemoglobin	0.294

Table A.1: Top 20 highest absolute Pearson correlations among numerical covariates.

*cholesterol* because it has a direct deterministic dependence on *HDL cholesterol* ( $Total = HDL + LDL + VLDL$ ). Including *total cholesterol* as a predictor would introduce a compositional relationship in which the predictor mathematically contains the outcome itself, leading to a mechanically induced association rather than an independent explanatory effect. After these adjustments, the highest remaining correlation is 0.568 between *MCH* and *MCHC*. Variance Inflation Factors (VIFs) indicate acceptable multicollinearity for all remaining numerical covariates, with all VIFs  $< 5$ .

We also examine associations among categorical covariates using asymptotic chi-squared tests for all pairwise combinations (Table A.2). The strongest associations (lowest  $p$ -values) emerge between *alcohol* and *sex* ( $\chi^2 = 70.91$ ,  $p < 2 \times 10^{-16}$ ), *physical activity* and *smoking* ( $\chi^2 = 27.89$ ,  $p = 8.81 \times 10^{-7}$ ), and *alcohol* and *smoking* ( $\chi^2 = 35.2$ ,  $p = 2.75 \times 10^{-3}$ ). We exclude from the analysis the variable *smoking* and *alcohol* due to the high percentage of missing values and their strong associations with other categorical covariates, such as *alcohol* with *sex* ( $\chi^2 = 70.91$ ,  $p < 2 \times 10^{-16}$ ), *physical activity* with *smoking* ( $\chi^2 = 27.89$ ,  $p = 8.81 \times 10^{-7}$ ), and *alcohol* with *smoking* ( $\chi^2 = 8.97$ ,  $p = 2.75 \times 10^{-3}$ ), which could introduce redundancy and complicate the interpretation of lifestyle effects.

We continue the exploratory data analysis by assessing the association between the target variables and the selected covariates to identify potentially uninformative predictors before model specification. For the numerical covariates, we compute the Pearson correlation  $r$  coefficient between

Variable Pair	$\chi^2$	df	p-value	Significant
<i>alcohol</i> vs Physical_activity	8.96	2	1.13e-02	Yes
Rh vs ABO	10.78	3	1.3e-02	Yes
<i>smoking</i> vs <i>sex</i>	5.00	1	2.53e-02	Yes
ABO vs <i>sex</i>	3.89	3	2.74e-01	No
<i>alcohol</i> vs <i>smoking</i>	8.97	1	2.75e-03	Yes
<i>smoking</i> vs Rh	0.96	1	3.26e-01	No
Physical_activity vs <i>sex</i>	2.15	2	3.41e-01	No
Physical_activity vs ABO	13.44	6	3.66e-02	Yes
<i>smoking</i> vs ABO	13.45	3	3.76e-03	Yes
Physical_activity vs Rh	1.25	2	5.35e-01	No
<i>alcohol</i> vs ABO	7.59	3	5.52e-02	No
Rh vs <i>sex</i>	7.69	1	5.54e-03	Yes
<i>alcohol</i> vs Rh	0.09	1	7.69e-01	No
Physical_activity vs <i>smoking</i>	27.89	2	8.81e-07	Yes
<i>alcohol</i> vs <i>sex</i>	70.91	1	< 2e-16	Yes

Table A.2: Chi-Squared tests for associations among categorical covariates.

each target and each variable (Table A.3). For categorical covariates, we rely on Kruskal–Wallis tests to evaluate differences in target distributions across groups (Table A.4). Based on these results, we exclude the categorical covariates *Rh* and *ABO*. Although some associations with the targets are statistically significant, they are generally weak and accompanied by associations with other categorical covariates (see Table A.2), suggesting limited additional explanatory value. After this screening step, we include the 18 numerical covariates reported in Table A.3 in the model. Among categorical variables, we include *sex*, given its consistently strong associations with all target variables (Table A.4), and *physical activity*, due to its relevance as a key lifestyle factor and its systematic association with metabolic outcomes.

Finally, we explore the associations between the remaining categorical and numerical covariates using Kruskal-Wallis tests (Table A.5) and boxplots (Figure A.4). These analyses reveal clear distributional shifts across *sex* for several numerical covariates and target variates. To account for such heterogeneity, we include interaction terms between *sex* and the numerical covariates highlighted in Figure A.4 in the final model specification. Additionally, we introduce the interaction between *sex* and *physical activity* to investigate better potential sex-specific lifestyle effects on MetS risk for men and women.

## A.2 Missing values in the covariates

The dataset contains missing values in several covariates (see Figure A.2). These are imputed using multiple imputation by chained equations (MICE) (Van Buuren and Groothuis-Oudshoorn, 2011) under a Fully Conditional Specification (FCS) framework (Van Buuren, 2012), with two-level predictive mean matching (2l.pmm) implemented in the add-on package `miceadds` (Robitzsch

	HDL	Waist_Circumference	<i>glucose</i>	<i>PMAX</i>	<i>triglycerides</i>
ALT	-0.176	0.259	0.046	0.087	0.227
Height	-0.208	0.278	-0.014	0.011	0.051
Basophils_pct	0.102	-0.046	-0.027	-0.015	-0.045
Creatinine	-0.169	0.156	0.024	0.032	0.134
Volume_distribution	0.049	0.056	0.004	0.097	-0.012
MCHC	-0.139	0.043	-0.051	0.006	0.073
Hemoglobin	-0.248	0.273	0.023	0.134	0.220
MCH	0.091	-0.073	-0.004	-0.052	-0.023
Eosinophils_pct	-0.023	0.022	-0.027	-0.023	0.020
Ferritin	-0.107	0.113	0.017	0.037	0.108
WBC	-0.140	0.169	0.035	0.071	0.207
Lymphocytes_pct	0.045	-0.050	-0.036	-0.099	-0.053
Monocytes_pct	0.013	0.021	-0.079	-0.025	-0.041
Platelets	0.047	0.020	0.016	0.025	0.039
Heart_rate	-0.074	0.081	0.041	0.132	0.091
Total_proteins	-0.038	0.034	0.011	-0.008	0.080
Age	0.073	0.233	0.137	0.303	0.107
BMI	-0.350	0.819	0.111	0.282	0.284

Table A.3: Pearson correlations: numerical covariates vs MetS targets.

Covariate	HDL	Waist_Circumference	<i>glucose</i>	<i>PMAX</i>	<i>triglycerides</i>
Physical_activity	<2e-16	<2e-16	1.6e-06	3.23e-07	<2e-16
Rh	4.63e-02	1.95e-01	1.26e-01	9.44e-01	3.31e-02
ABO	4.91e-04	2.28e-03	4.08e-02	4.54e-02	1.69e-04
<i>sex</i>	<2e-16	<2e-16	8.87e-07	<2e-16	<2e-16

Table A.4: Kruskal-Wallis p-values: categorical covariates vs METs targets.

Numerical covariate	<i>physical activity</i>	<i>sex</i>
ALT	4.45e-04	<2e-16
Height	2.4e-01	<2e-16
Basophils_pct	1.03e-05	3.96e-02
Creatinine	2.39e-01	<2e-16
Volume_distribution	4.81e-01	<2e-16
MCHC	2.25e-01	<2e-16
Hemoglobin	6.56e-03	<2e-16
MCH	4.22e-05	1.29e-01
Eosinophils_pct	4.48e-02	<2e-16
Ferritin	3.56e-01	<2e-16
WBC	2.76e-13	2.37e-01
Lymphocytes_pct	1.74e-02	<2e-16
Monocytes_pct	7.76e-03	<2e-16
Platelets	3.6e-01	<2e-16
Heart_rate	1.49e-10	2.4e-07
Total_proteins	1.88e-02	7.36e-15
Age	2.34e-03	<2e-16
BMI	<2e-16	<2e-16

Table A.5: Kruskal-Wallis p-values: continuous responses vs categorical covariates.

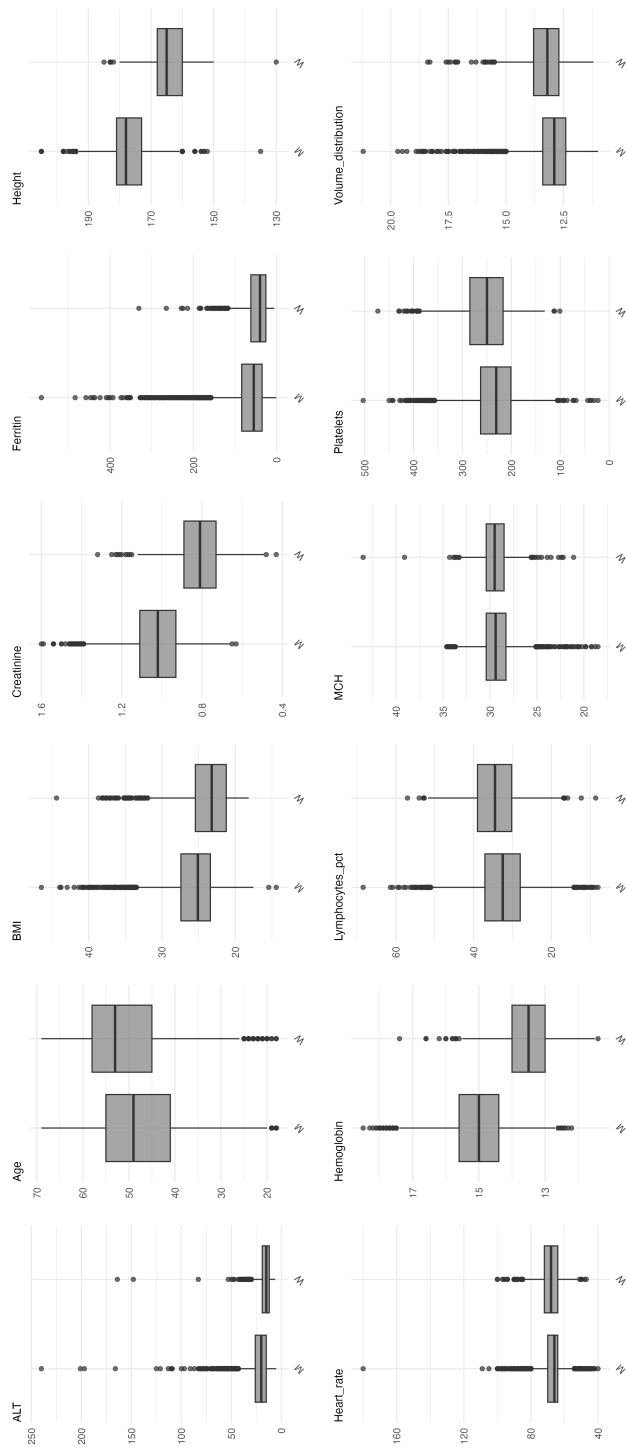


Figure A.4: Boxplots of numerical covariates grouped by *sex*.

et al., 2021). Donor ID is specified as the level-2 clustering variable to account for the longitudinal structure of repeated measurements.

Variables excluded from our Bayesian model (as explained above), such as *ABO* and *Rh*, are retained as auxiliary predictors in the imputation procedure to improve the estimation of missing-value distributions. The target variables were intentionally excluded as predictors in the imputation models to avoid inducing spurious relationships between the outcomes and the covariates. The MICE algorithm is run for 10 iterations.

### A.3 Missing values in *waist circumference*

For donor  $i$  at visit  $j$  with missing *waist circumference*, the corresponding log *waist circumference*  $Y_{ij}^{(k)}$  (where  $k = \textit{waist circumference}$ ) is treated as an additional model parameter and assigned an improper uniform prior  $Y_{ij}^{(k)} \sim \text{Uniform}(-\infty, \infty)$ ; recall that the model is specified on the log scale. The distribution from which the missing value is sampled is the full conditional:

$$Y_{ij}^{(k)} | \mathbf{Y}_{ij,-k}, \boldsymbol{\mu}_{ij}, \boldsymbol{\Sigma}_Y \sim \mathcal{N}(\mu_{ij}^{(k)} + \boldsymbol{\Sigma}_{k,-k} \boldsymbol{\Sigma}_{-k,-k}^{-1} (\mathbf{Y}_{ij,-k}^{\text{obs}} - \boldsymbol{\mu}_{ij,-k}), \Sigma_{kk|-k}),$$

where  $\mathbf{Y}_{ij,-k}$  denotes the vector of observed components of  $\mathbf{Y}_{ij}$  excluding the  $k$ -th element,  $\boldsymbol{\mu}_{ij,-k}$  is the corresponding subvector of mean parameters,  $\boldsymbol{\Sigma}_{-k,-k}$  is the submatrix of  $\boldsymbol{\Sigma}_Y$  excluding the  $k$ -th row and column,  $\boldsymbol{\Sigma}_{k,-k}$  is the vector of covariances between the  $k$ -th component and the remaining components, and  $\Sigma_{kk|-k}$  denotes the conditional variance of  $Y_{ij}^{(k)}$ . This approach allows joint estimation of regression parameters and imputation of missing values within the Bayesian framework, avoiding the separate or sequential reuse of the data.

## B Appendix

### B.1 Multivariate t-CAR model

To further investigate potential temporal dependencies, we have extended our baseline multivariate mixed-effects model (1)–(6) to explicitly account for the unequally spaced longitudinal nature of the donations. Specifically, we incorporated a Continuous Autoregressive (t-CAR) structure (Diggle, 1988). For each donor  $i$  and each target variable  $k$ , the linear predictor at any subsequent visit  $j > 1$  is updated to include an autoregressive term of  $Y_{i,j-1}^{(k)}$  that decays exponentially with the time  $\Delta t_{ij}$ , measured in years, elapsed since the previous visit:

$$\mu_{ij}^{(k)} = \mathbf{x}_{ij}' \boldsymbol{\beta}^{(k)} + b_i^{(k)} + \exp(-\phi^{(k)} \Delta t_{ij}) Y_{i,j-1}^{(k)}.$$

Here,  $\phi^{(k)} \geq 0$  represents the target-specific decay rate of the temporal autocorrelation. To ensure positivity, we assume a weakly informative Gamma prior to these parameters, specifically  $\phi^{(k)} \stackrel{\text{iid}}{\sim} \text{Gamma}(2, 0.2)$ ,  $k = 1, 2, \dots, 5$ .

Table B.1 reports the posterior summaries for the decay rate parameters  $\phi^{(1)}, \dots, \phi^{(5)}$ . The

Target Variable	Median	Mean	95% CI Lower	95% CI Upper
<i>PMAX</i> $\phi^{(1)}$	14.97	16.15	10.60	28.91
<i>HDL cholesterol</i> $\phi^{(2)}$	18.60	19.95	13.08	34.68
<i>glucose</i> $\phi^{(3)}$	19.03	20.48	12.55	36.69
<i>triglycerides</i> $\phi^{(4)}$	23.95	25.32	15.95	42.36
<i>waist circumference</i> $\phi^{(5)}$	24.36	25.94	14.27	45.33

Table B.1: Posterior summaries of the decay rate parameters  $\phi^{(1)}, \dots, \phi^{(5)}$  from the multivariate t-CAR model.

posterior estimates of  $\phi^{(1)}, \dots, \phi^{(5)}$  are notably high across all five target variables. In the context of a t-CAR process, such values indicate that the correlation between consecutive measurements drops toward zero extremely quickly. To provide the most conservative assessment, we can evaluate the residual autocorrelation  $\exp(-\phi^{(k)} \Delta t_{ij})$  using the lower bounds of the 95% credible intervals (i.e., the slowest estimated decay rates). For systolic blood pressure, which exhibits the lowest overall bound ( $\phi \approx 10.61$ ), autocorrelation after just three months ( $\Delta t = 0.25$ ) is only  $\approx 0.071$  (roughly 7%). After six months ( $\Delta t = 0.5$ ), it drops to negligible  $\approx 0.005$ . Instead, for *triglycerides*, which presents the highest lower bound ( $\phi \approx 15.96$ ), the autocorrelation plummets to  $\approx 0.018$  after three months and is virtually zero ( $\approx 0.0003$ ) after six months.

Given that the sample average interval between consecutive visits is 291 days for men and 339 days for women, the resulting autocorrelation factor becomes negligibly small for all practical purposes, even under the most conservative posterior bounds. These results confirm that temporal autocorrelation is entirely negligible once the relevant covariates and donor-specific random intercepts are accounted for. Consequently, the continuous autoregressive component was omitted from the final multivariate specification to preserve model parsimony and maintain computational efficiency.

## B.2 Univariate t-CAR models

We have also investigated potential temporal dependencies by fitting five independent univariate mixed-effects models. Following the same rationale described for the multivariate case (Section B.1), each univariate model has been extended with a t-CAR structure in the likelihood, applying the identical Gamma(2,0.2) prior to the target-specific decay rate parameters  $\phi^{(k)}$ ,  $k = 1, 2, \dots, 5$ .

Table B.2 reports the posterior summaries for the decay parameters estimated by these independent models. Posterior inference is highly consistent with the multivariate model estimates.

Target Variable	Median	Mean	95% CI Lower	95% CI Upper
<i>P</i> MAX $\phi^{(1)}$	15.37	16.62	10.88	30.08
<i>HDL cholesterol</i> $\phi^{(2)}$	21.44	23.04	14.89	34.33
<i>glucose</i> $\phi^{(3)}$	19.44	20.86	12.72	37.53
<i>triglycerides</i> $\phi^{(4)}$	21.80	23.11	14.11	39.79
<i>waist circumference</i> $\phi^{(5)}$	25.53	26.66	14.91	45.84

Table B.2: Posterior summaries of the decay rate parameter  $\phi$  from the independent univariate t-CAR models.

The estimated decay rates remain notably high across all five independently fitted models. Applying the same conservative assessment on the lower bounds of the 95% credible intervals, the slowest decay is observed for systolic blood pressure *P*MAX ( $\phi^{(1)} \approx 10.88$ ). Even in this worst-case scenario, the residual autocorrelation drops to  $\approx 0.066$  after three months ( $\Delta t = 0.25$ ) and is practically zero ( $\approx 0.004$ ) after six months ( $\Delta t = 0.5$ ). For the highest lower bound (*waist circumference*,  $\phi^{(5)} \approx 14.91$ ), the autocorrelation falls to  $\approx 0.024$  at three months.

Considering the average intervals between donations, these univariate analyses independently corroborate that temporal autocorrelation vanishes well before the subsequent visit. This provides further solid justification for omitting the autoregressive component in the final model specifications.

### B.3 Predictive performance and model selection

To formally justify the adoption of the joint multivariate framework without the autoregressive component, we compare the out-of-sample predictive performance of the evaluated specifications using the Leave-One-Out Information Criterion (LOOIC) (Vehtari et al., 2017) and the Watanabe-Akaike Information Criterion (WAIC) (Watanabe, 2010). For the independent univariate framework described in Section B.2, the total information criteria were calculated as the sum of the individual models' values, with the aggregated standard errors (SE) computed as the square root of the sum of the squared individual standard errors. Lower values of WAIC and LOOIC indicate better model fit. Table B.3 summarizes the predictive performance metrics. Our Bayesian multivariate model described by (1)–(6) in Section 3 yields a drastically lower LOOIC (74,769.6) compared to the aggregated independent univariate models (139,309.5). This massive improvement in predictive accuracy is primarily driven by the joint model's ability to borrow strength across the correlated metabolic targets. Specifically, the multivariate structure drastically reduces the uncertainty in imputing the highly prevalent missing values for *waist circumference* by dynami-

Model Specification	WAIC	(SE)	LOOIC	(SE)
Independent Univariate Models (Sum)	137,904.7	(1,745.6)	139,309.5	(1,484.8)
Multivariate t-CAR Model	71,838.1	(462.8)	74,862.9	(459.9)
<b>Multivariate Baseline Model</b>	<b>71,773.2</b>	<b>(464.2)</b>	<b>74,769.6</b>	<b>(461.9)</b>

Table B.3: Comparison of out-of-sample predictive performance metrics across the modeling frameworks. The LOOIC is approximated using the Pareto-smoothed importance sampling method.

cally leveraging the concurrent observed levels of *glucose*, *triglycerides*, blood pressure, and *HDL cholesterol*, through the estimates of the residual and random-effect covariance matrices,  $\Sigma_t$  and  $\Sigma_b$ .

Furthermore, when comparing the multivariate formulations, the inclusion of the t-CAR component (Section B.1) does not yield any predictive gain. The LOOIC for the t-CAR model (74,862.9) is slightly higher than that of the final simpler specification in (1)–(6) (74,769.6). The difference in LOOIC between these two models ( $\approx 93$ ) is substantially smaller than their respective standard errors ( $\approx 460$ ), indicating that the models are practically indistinguishable in terms of expected predictive accuracy. This minor increase effectively reflects a penalization for the inclusion of unnecessary autoregressive parameters without any corresponding improvement in fit. The WAIC values perfectly mirror this behavior.

These predictive performance metrics, coupled with the rapid decay of the temporal correlation parameters  $\phi^{(k)}$  discussed in Sections B.1, B.2, confirm that the multivariate mixed-effects likelihood (1)–(2) represents a flexible and parsimonious model for this dataset.

## C Appendix

### C.1 Simulation design

To further evaluate the predictive performance of our multivariate Bayesian framework, we have designed a simulation study that emulates the longitudinal dynamics of the AVIS Milan blood donor cohort while imposing controlled temporal dependencies.

The simulation study design assumes three biomarkers measured at different visits, *BMI*, *age*, and *sex*, which are central determinants across the five MetS biomarker outcomes in the real-case application. Age at each visit is included as a time-varying covariate (as *BMI*), allowing the model to account for calendar time across donations. We have simulated a cohort of  $N = 50$  donors (43 males, 7 females), each observed at five consecutive visits equally spaced over time. To mimic the AVIS Milan longitudinal structure for which the average gap time is approximately 10 months, visits have been assumed to occur every 12 months for all donors.

To preserve biological realism, the continuous covariates  $BMI$  and  $age$  at the beginning of the study have been sampled directly from the gender-specific empirical distributions of the real-case dataset. For donors aged  $\geq 50$  years, the longitudinal trajectory of  $BMI$  has been modeled as a random walk with a deterministic drift, reflecting the physiological weight gain often observed in older populations. Specifically, for donor  $i$  at visit  $j$ , we have simulated:

$$BMI_{i,j} = \begin{cases} 1.05 \cdot BMI_{i,j-1} + \epsilon_{i,j}^{BMI} & \text{if } age_{i,j} \geq 50 \\ BMI_{i,j-1} + \epsilon_{i,j}^{BMI} & \text{otherwise} \end{cases},$$

where  $\epsilon_{i,j}^{BMI} \stackrel{\text{iid}}{\sim} \mathcal{N}(0, 0.36)$  represents the inter-visit measurement noise.

The five MetS biomarkers, denoted by the vector  $\mathbf{Y}_{i,j}$ , have been simulated in a log-standardized space. To explicitly test the model’s capacity to handle temporal autocorrelation, we have generated the latent outcomes via a first-order autoregressive AR(1) process, with a persistence parameter  $\rho = 0.5$ . This relatively high degree of autocorrelation has been deliberately chosen to challenge the model under conditions of strong temporal stability. The generation process is as follows:

$$\mathbf{Y}_{i,j} = \mathbf{x}_{i,j}^\top \boldsymbol{\beta} + \rho \mathbf{Y}_{i,j-1} + \sigma \cdot \boldsymbol{\epsilon}_{i,j}$$

To introduce heavier tails in the simulated responses, the error term  $\boldsymbol{\epsilon}_{i,j}$  has been sampled from a Student’s  $t$ -distribution with  $\nu = 4$  degrees of freedom, rather than from a Gaussian distribution. The scale parameter  $\sigma$  has been set to 3 to generate moderate variability in the simulated biomarkers while preserving realistic separation between low- and high-risk profiles.

## C.2 Predictive evaluation

We consider simulated observations from the first 4 visits for each donor as the training set, and test the predictive accuracy of the traffic-light warning system. (Section 4) at the fifth visit (ground truth). Using the empirical prevalence ( $t = 0.11$ ) as the classification threshold, we report the system’s performance on the simulated test set in Table C.1. The model successfully identifies

<b>Traffic-light classification</b>	True No	True Yes
Green	28	2
Yellow	9	2
Red	5	4

Table C.1: Confusion matrix: traffic-light classification on (simulated) data from the 5th visit.

75% of future MetS cases (6 out of 8 true cases), categorizing them as either high risk (Red) or potential risk (Yellow). Furthermore, the model maintains robust specificity in the Green category,

correctly classifying 66.7% (28 out of 42) of the healthy donors. These results show that the proposed framework achieves reasonable predictive accuracy despite relevant temporal dependence and model misspecification.